Title: 3_D surface stereometry of Ag/DLC nanocomposite prepared by RF-PECVD

Author: Sebastian Stach, Ştefan Ţălu, Senour Abdolghaderi, Azizollah Shafiekhani, Jahangir Bahmanie

Citation style: Stach Sebastian, Ţălu Ştefan, Abdolghaderi Senour, Shafiekhani Azizollah, Bahmanie Jahangir. (2019). 3_D surface stereometry of Ag/DLC nanocomposite prepared by RF-PECVD. “Results in Physics” (Vol. 15, 2019, art. no .102731, s. 1-8), DOI: 10.1016/j.rinp.2019.102731

Results in Physics 15 (2019) 102731

Contents lists available at ScienceDirect

Results in Physics

journal homepage: www.elsevier.com/locate/rinp

3_D surface stereometry of Ag/DLC nanocomposite prepared by RF-PECVD

Sebastian Stach[a], Ştefan Ţălu[b], Senour Abdolghaderi[c,d,*], Azizollah Shafiekhani[c], Jahangir Bahmani[e]

[a] University of Silesia, Faculty of Computer Science and Materials Science, Institute of Informatics, Department of Biomedical Computer Systems, Będzińska 39, 41-205 Sosnowiec, Poland
[b] Technical University of Cluj-Napoca, The Directorate of Research, Development and Innovation Management (DMCDI), 15 Constantin Daicoviciu St., Cluj-Napoca, 400020 Cluj County, Romania
[c] Alzahra University, Physics Department, Tehran, Iran
[d] Department of Education of Kurdistan Provience, Sanandaj, Iran
[e] Department of Physics, College of Science, University of Raparin, Iraq

ARTICLE INFO

Keywords:
Ag/DLC nanocomposite
Atomic force microscopy
RF-PECVD
Stereometric analysis
Surface microtexture

ABSTRACT

In this study, a stereometric analysis of the three-dimensional (3-D) surfaces of the Ag/diamond-like carbon (DLC) nanocomposite films was done. The nanocomposite thin films were fabricated by Radio Frequency Plasma-Enhanced Chemical Vapour Deposition (RF-PECVD). The 3-D surface microtexture was studied by high-resolution Atomic Force Microscopy (AFM) records combined with statistical analyses. More detailed information about surface statistical parameters and topographic features of analyzed samples were performed. The statistical parameters relating to the segmented motifs consistent with ISO 25178-2: 2012 have been generated using MountainsMap® Premium software. The analysis was performed by modeling Ag/DLC nanocomposite surface microtexture based on motif analysis (detection of essential characteristics in terms of surface dimensions, volume, curvature, shape) to be included in computer interactive simulation algorithms.

Introduction

Recent advances in micro/nano manufacturing of Ag/DLC nanocomposite films have been considered in various theoretical and experimental approaches in nanotechnology.

Marciano et al. [1] studied the antibacterial activity of DLC, Ag–DLC and silver colloidal solution by bacterial eradication tests with Escherichia coli (E. coli) at various incubation times. They demonstrated that the total compressive stress decreased extensively with the increase of silver nanoparticle layers in Ag–DLC.

Wu et al. [2] prepared Ag/DLC thin films by medium frequency unbalanced magnetron sputtering method. They found that the Ag concentration increased with the increasing Ar/CH_4 ratios, accompanied by the increasing number and size of Ag crystalline.

Hybrid RF/MS PACVD (radio frequency/magnetron sputtering plasma assisted chemical vapour deposition) technique was applied by Bociaga et al. [3] to evaluate antimicrobial efficacy and biocompatibility of gradient a-C:H/Ti + Ag coatings concerning the surface physicochemical properties and chemical composition of the coating.

Baba et al. [4] prepared Ag/DLC thin films on austenitic type stainless steel SUS316L and silicon wafer substrates by a process combining reactive magnetron sputtering with plasma source ion implantation (PSII) to study its antibacterial activity using Staphylococcus aureus bacteria.

Constantinou et al. [5] used pulsed laser deposition (PLD) with an excimer laser technique to obtain different DLC:Ag films. They studied the morphological, topographical, crystallographic, compositional and mechanical/tribological characteristics of these films.

The electrical percolation threshold in Ag/DLC nanocomposite films was studied by Abdolghaderi et al. [6]. They used the RF-sputtering method to deposit Ag nanoparticle in the DLC matrix on glass and silicon substrates.

Detailed information about 3-D surface microtexture at the micro/nanoscale has important implications in the rational design and optimization in engineering applications and provides new opportunities for the investigation of precise topographical, spatial and chemical properties [7–11].

The numerical analysis according to stereometric parameters of the 3-D surface microtexture can be realized with a minimal set of criteria and surface parameters [12–16].

Atomic Force Microscopy (AFM) enables the characterization of the nanoscale surface in different environments and creates 3-D topographic images to find out surface spatial complexity [17–20]. The

* Corresponding author.
E-mail addresses: sebastian.stach@us.edu.pl (S. Stach), s.abdolghaderi@gmail.com (S. Abdolghaderi), ashafie@theory.ipm.ac.ir (A. Shafiekhani).

https://doi.org/10.1016/j.rinp.2019.102731
Received 7 April 2019; Received in revised form 4 October 2019; Accepted 5 October 2019
Available online 15 October 2019

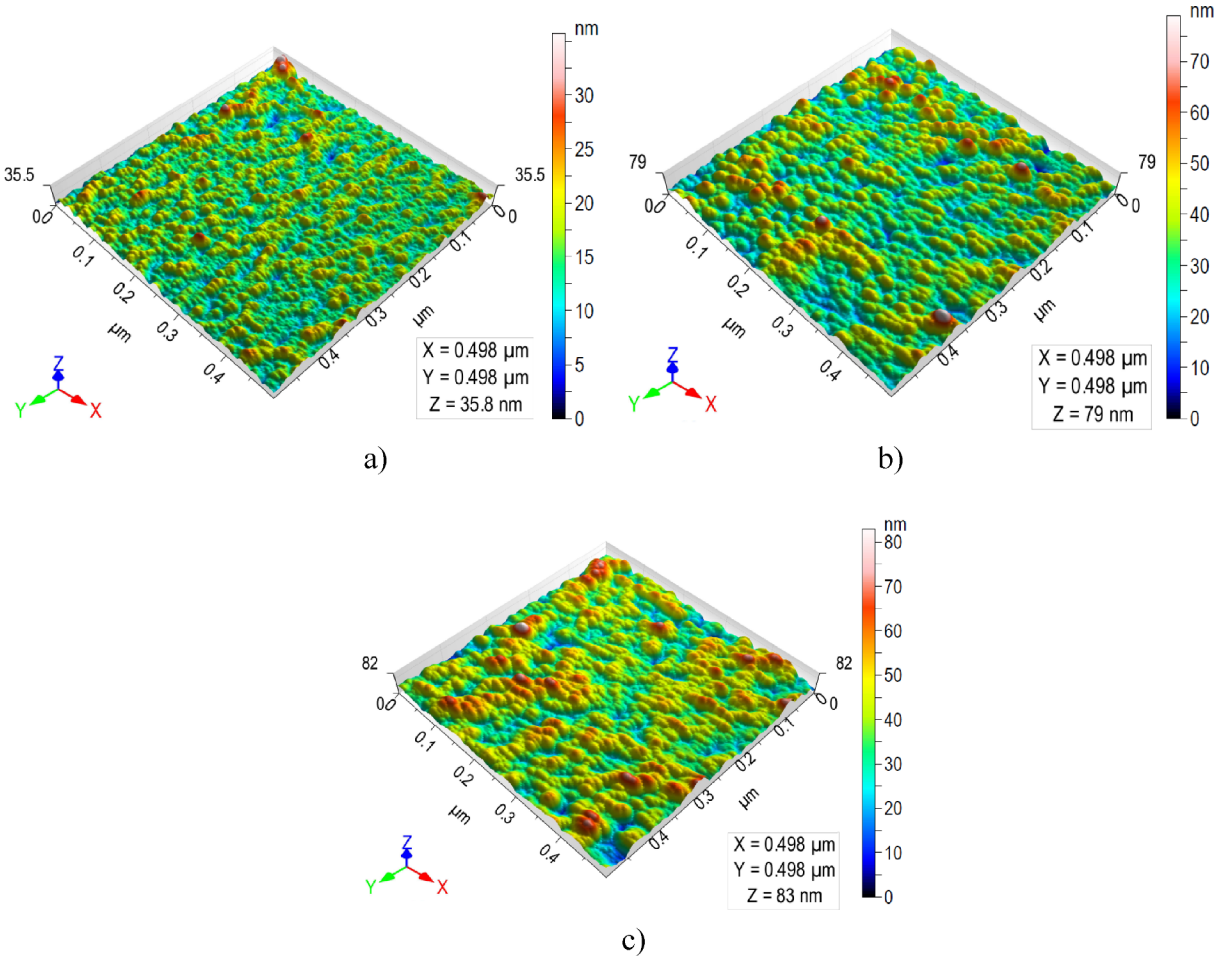

Fig. 1. Relevant 3-D AFM micrographs of samples: a) #1, b) #2, and c) #3.

integration of AFM records with image processing techniques makes it possible to obtain information about a 3-D pattern of complex surfaces [21–25].

The aim of this study is to synthesise the Ag/DLC nanocomposite with different deposition time by RF-PECVD and to indicate the 3-D surface morphology using AFM and statistical parameters, in accordance with ISO 25178-2: 2012 [26].

Methods

Materials and synthesis

In this study the Ag/DLC thin films were fabricated by sputtering and RF-PECVD technique at the room temperature. Glass and silicon substrates (1 cm × 1 cm) located on the holder as the lower electrode in a steel chamber and a pure silver target (5 cm diameter) connected to RF power as the upper electrode. The distance between electrodes was 4 cm. Laboratories acetylene gas (precursor) as operating gas was entered into the reaction chamber for ionization and formation of plasma to the dispersion of nanoparticles from the target silver to start deposition of hydrogenated carbon with Ag nanoparticle on the substrate with a constant rate. The initial pressure of the chamber was 4 Pa.

Plasma is created by applying the radio frequency power between the electrodes where is filled by the precursor gas (acetylene). Electrons are started decomposing precursor gas molecules and exerting a large number of free radicals in the environment, also making ion targeting of silver possible. The RF power and bias voltages were 60 W and 80 V, respectively.

Deposition time and pressure in the chamber varied that chamber pressure was out of control during the deposition process. Three samples with 10 min, 25 min, and 40 min deposition time were used in this study and named as sample number #1, #2 and #3, respectively.

Results

AFM measurements

The AFM images of samples were obtained by atomic force microscopy (SPM system Solver P47H-PRO, Russia) in contact mode. The VIT_P_C-A/15 tip was used with the following grating description: typical resonant frequency 16 kHz, typical force constant 0.3 N/m and Al reflective coating. The scanning process was done with 10 mm per min and Image Processing and Data Analysis v2.1.15 software was used for data analyses.

Characterization of 3-D surface morphology was performed by stereometric analyses of AFM images. The relevant AFM images of thin films are shown in Fig. 1.

The motif analysis and watershed segmentation of the thin film 3-D surface microtexture

MountainsMap® Premium software version 6.2.7200 [27] was used

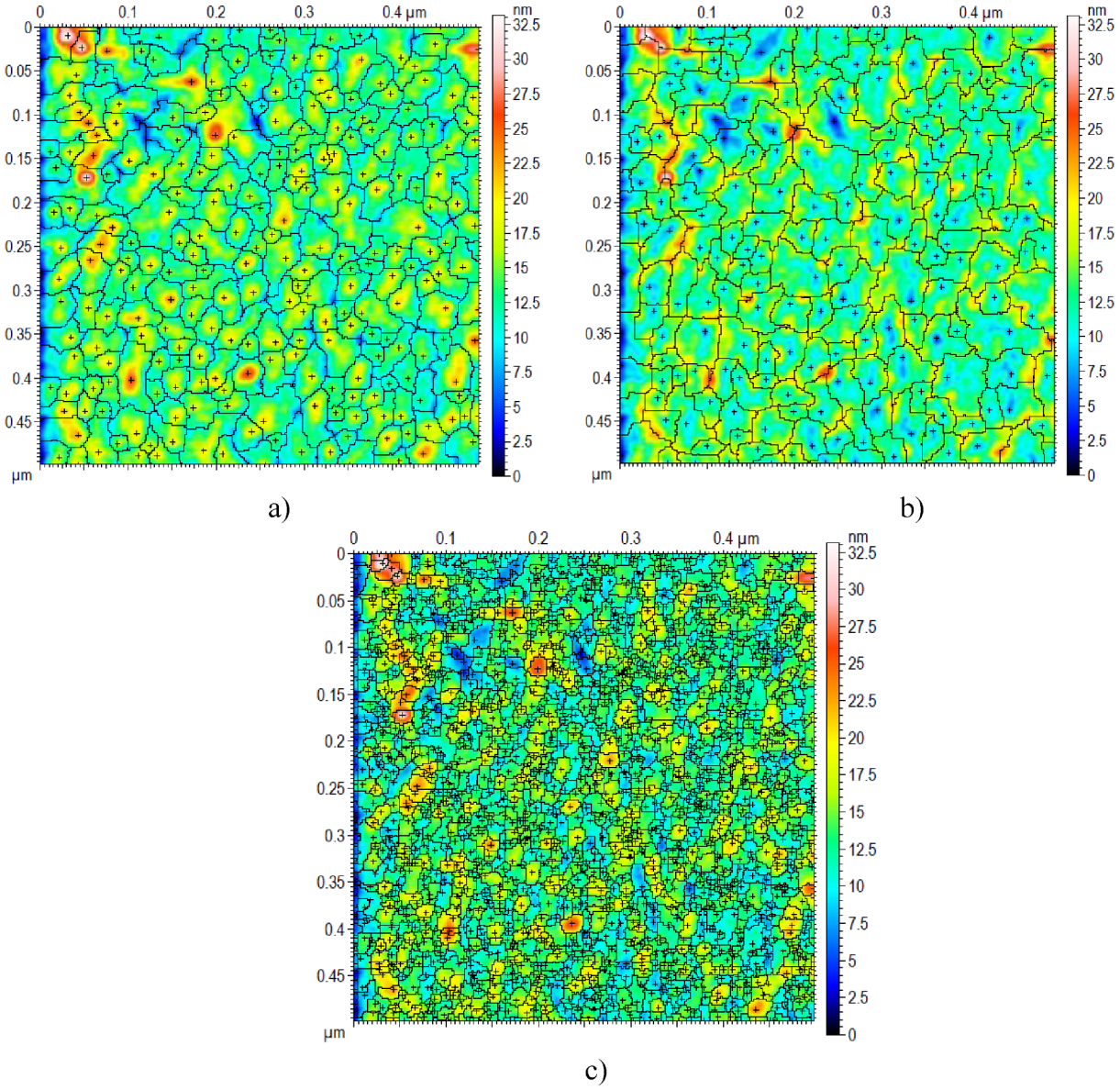

Fig. 2. The surface segmentation for the sample surface #1: a) peaks, b) pits, and c) shapes.

for the stereometric analysis of AFM images. The watershed segmentation method was applied to AFM images to determine surface features as pits or peaks, hill or dales and passages or watercourse lines by motif analyses (Figs. 2–4). The following segmentation options were applied in stereometric analysis: preprocessing with filter size 3 × 3; threshold: minimum height of motifs 5% of Sz; minimum area of motifs 0.010% of the surface area.

The obtained statistical surface parameters are specified in Tables 1–3.

The power spectrum density (PSD) analysis of the thin film 3-D surface microtexture

Power spectral density shows the strength of the signal in the frequency domain. The 1D PSD (Power Spectrum Density) average functions calculate PSD spectra for each X line or Y column and the corresponding average PSD spectrum graphs were computed using SPIP™ 6.7.4 software [28].

In Fig. 5 are shown these computed functions for the average X-PSD profile (a, b, c) and the average Y-PSD profile (d, e, f).

Discussion

Accurate characterization of 3-D surface morphology by AFM images and statistical surface parameters with a description of the topography determines the pattern of spatial distribution in analyzed Ag/DLC nanocomposite thin films.

The following parameters reflect the surface roughness and heterogeneity. Small vertical deviations of the surface roughness from the mean line reveal a smoother profile. It can be noted that all samples have a smooth surface due to the valuable fabrication procedure with characteristic fractal features.

Segmented peaks

The number of motifs composed of peaks is 251 for sample #1, 181

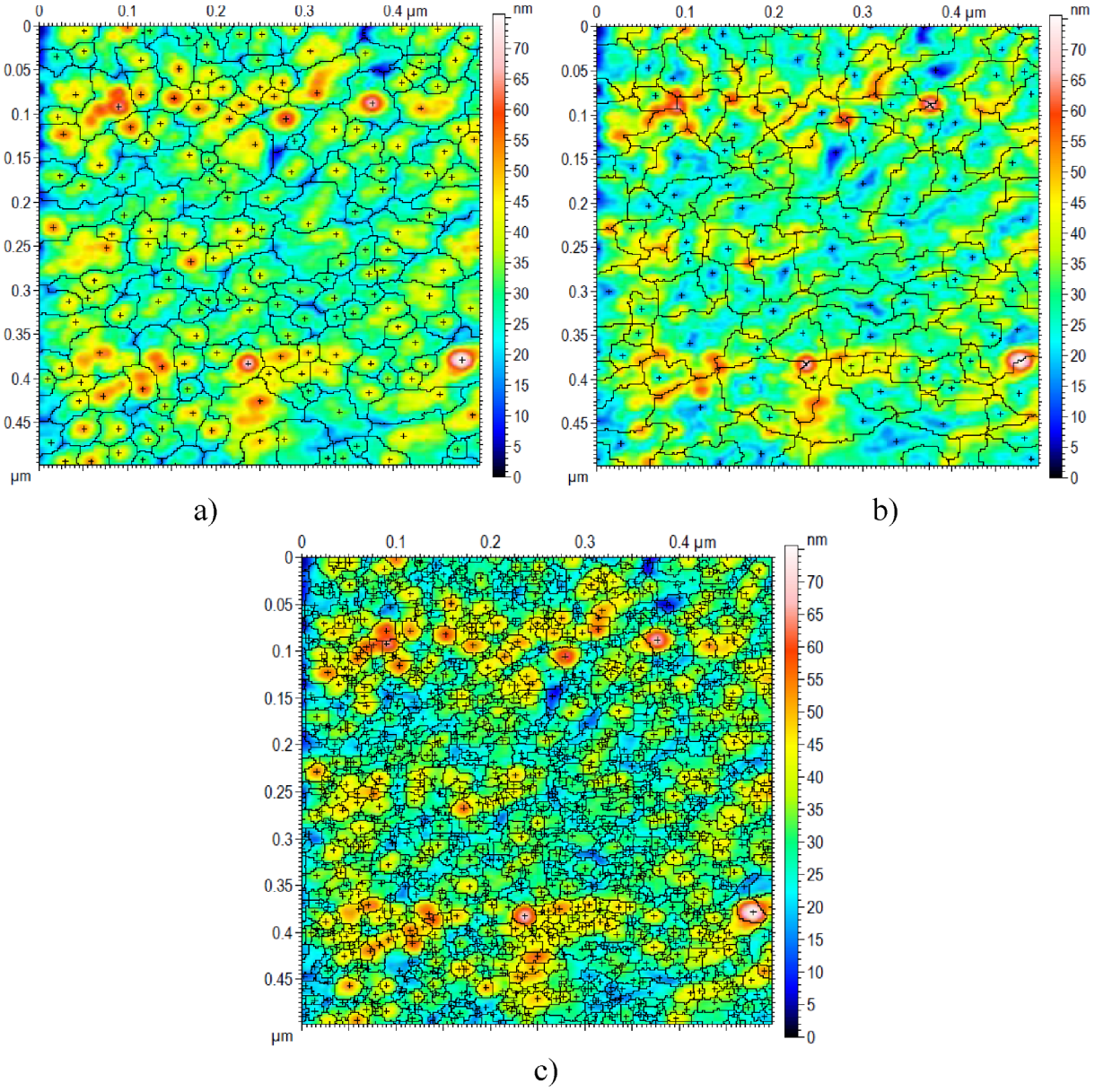

Fig. 3. The surface segmentation for the sample surface # 2: a) peaks, b) pits, and c) shapes.

and 134 for samples #2 and #3, respectively. The mean height parameter is 3.70 nm for sample #1, 9.21 nm for sample #2 and the highest value 9.24 nm for sample #3. The mean area of the motifs composed of peaks is 996 nm^2, 1381 nm^2 and 1870 nm^2 for sample #1, #2 and #3, respectively. The third sample has the highest mean volume of material in motifs (2709 nm^3), whereas for sample #2 is 2221 nm^3, and the lowest value was of sample #1 (546 nm^3), nearly fifth of mean volume of the third sample.

The parameter means the perimeter of peaks increases from a minimum value of 131 nm (sample #1), to the medium value of 156 nm (sample #2), while a maximum value of 185 nm is found for sample #3.

The mean of equivalent diameters of peaks is increased from 32 nm to 44.4 nm in the same way.

The mean of minimum diameter angles decreases from -8.49° (sample #1) to -20.9° (sample #2), whereas the lowest value of -22.8° was found for sample #3. Also, the mean of maximum diameter angles parameter has the lowest value of -23° for sample #1, the highest value of -13.9° for sample #2, and an average value of -17.1° for sample #3.

The highest mean form factor belongs to sample #1 (0.617) and the smallest to sample #3 (0.593) that it means the motif was decreased with time deposition increasing.

The mean aspect ratio parameter has the same value 2.20 for both samples #1 and #2, and a bigger value of 2.26 for sample #3; all three samples have an elongated shape.

The lowest value of the mean roundness of samples is 0.520 (sample #3) and the highest value is 0.544 (sample #2). Additionally, the lowest value of the mean compactness parameter belongs to sample #1 (0.727) and the highest value belongs to sample #2 (0.732); consequently, the grains are elongated. The maximum value of the mean orientation belongs to sample #2 (81°), the minimum value is 66.4° for sample #3, and sample #1 has a medium value of 73.5°.

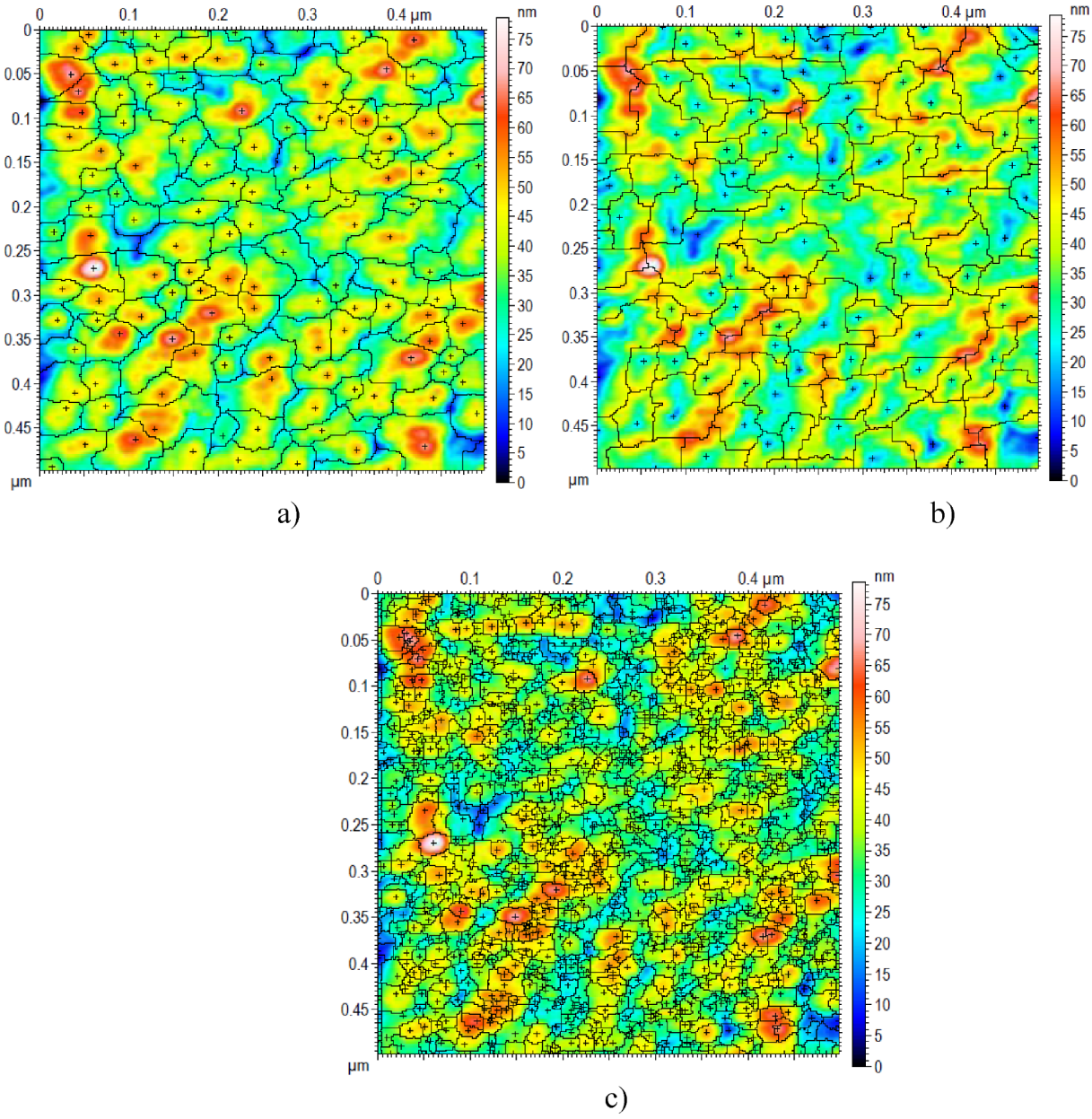

Fig. 4. The surface segmentation for the sample surface #3: a) peaks, b) pits, and c) shapes.

Table 1
Parameter values for different measurement data resulting from the surface segmentation of sample # 1 (associated with Fig. 2).

Sample # 1 Parameter	The peaks	The pits	The shapes
Number of motifs	251	188	1545
Mean height [nm]	3.70	3.23	13.3
Mean area [nm^2]	996	1330	162
Mean volume [nm^3]	546	431	48.7
Mean perimeter [µm]	0.131	0.158	0.0473
Mean of equivalent diameters [µm]	0.032	0.0373	0.0115
Mean of mean diameters [µm]	0.031	0.0363	0.0112
Mean of minimum diameters [µm]	0.0213	0.0251	0.0068
Mean of maximum diameters [µm]	0.0444	0.052	0.0172
Mean of minimum diameter angles [°]	−8.49	−12.5	−33
Mean of maximum diameter angles [°]	−23	−22.2	−27.6
Mean form factor	0.617	0.572	0.623
Mean aspect ratio	2.20	2.18	2.84
Mean roundness	0.538	0.526	0.474
Mean compactness	0.727	0.722	0.682
Mean orientation [°]	73.5	77.9	79.5

Table 2
Parameter values for different measurement data resulting from the surface segmentation of sample # 2 (associated with Fig. 3).

Sample # 2 Parameter	The peaks	The pits	The shapes
Number of motifs	181	124	1284
Mean height [nm]	9.21	8.41	30.8
Mean area [nm^2]	1381	2020	195
Mean volume [nm^3]	2221	1574	125
Mean perimeter [µm]	0.156	0.203	0.053
Mean of equivalent diameters [µm]	0.0377	0.046	0.0129
Mean of mean diameters [µm]	0.0364	0.0442	0.0124
Mean of minimum diameters [µm]	0.0253	0.0296	0.0077
Mean of maximum diameters [µm]	0.0526	0.0666	0.0191
Mean of minimum diameter angles [°]	−20.9	−15	−35
Mean of maximum diameter angles [°]	−13.9	−13	−21.5
Mean form factor	0.612	0.531	0.613
Mean aspect ratio	2.20	2.41	2.85
Mean roundness	0.544	0.500	0.476
Mean compactness	0.732	0.701	0.683
Mean orientation [°]	81.0	80.4	82.1

Table 3
Parameter values for different measurement data resulting from the surface segmentation of sample # 3 (associated with Fig. 4).

Sample # 3 Parameter	The peaks	The pits	The shapes
Number of motifs	134	105	1114
Mean height [nm]	9.24	9.60	35.8
Mean area [nm^2]	1870	2380	224
Mean volume [nm^3]	2709	2227	127
Mean perimeter [μm]	0.185	0.216	0.0576
Mean of equivalent diameters [μm]	0.0444	0.0496	0.0138
Mean of mean diameters [μm]	0.0427	0.0479	0.0134
Mean of minimum diameters [μm]	0.030	0.032	0.0083
Mean of maximum diameters [μm]	0.0633	0.0701	0.0208
Mean of minimum diameter angles [°]	−22.8	−9.8	−36.9
Mean of maximum diameter angles [°]	−17.1	−15.4	−21.8
Mean form factor	0.593	0.553	0.604
Mean aspect ratio	2.26	2.33	2.90
Mean roundness	0.520	0.514	0.467
Mean compactness	0.716	0.712	0.676
Mean orientation [°]	66.4	81.9	84.8

Segmented pits

The obtained results of the segmentation of pits are analogous to those of peaks. In this case, a descending order in the number of motifs from sample #1 (1 8 8) to sample #3 (1 0 5) is observed too.

The mean height parameter of pits has the highest value of 9.6 nm for sample #3 and the lowest value of 3.23 nm for sample #1. Also, the mean area of pits has the highest value of 2380 nm^2 for the third sample and 1330 nm^2 for the first sample, the same order as in peak segmentation.

The mean volume and the mean perimeter of motifs parameters have similar increments. So, the mean volume and the mean perimeter of the first sample are 431 nm^3 and 158 nm respectively; the largest values belong to the third one (2227 nm^3 and 0.216 nm), whereas the average values belong to the second sample (1574 nm^3 and 203 nm). Like previous order, the mean of equivalent diameter has the lowest value for the first sample (37.3 nm), a medium value of 46 nm for the second sample and the highest value for the third sample (49.6 nm). The mean of mean diameter of pits is 36.3 nm, 44.2 nm and 47.9 nm for samples #1, #2 and #3 respectively.

In the case of the mean of minimum diameter angle, the highest value belongs to the second sample (−15°) and the lowest value belongs to the third one (−9.8°) and for the first sample is −12.5°.

The mean maximum diameter angle parameter has the highest value for the first sample (−22.2°), whereas the lowest value is for the second one (−13°).

The mean form factor parameter for sample #1 has the highest value (0.572), the lowest value (0.531) for the second sample, whereas the third sample has a middle value (0.553). Neither of them is close to 1 that means their shapes are elongated.

The mean of roundness and the mean of compactness have similar increments; the highest values belong to sample #1 (0.526, 0.722), the middle values belong to sample #3 (0.514, 0.712) and the lowest value belongs to sample #2 (0.500, 0.701).

The mean orientation parameter's values increase from sample #1 to sample #3, having the following values (77.9 – sample#1, 80.4 – sample #2 and 81.9 – sample #3).

Segmented shapes

The number of motifs segmented based on the shape has the highest value for sample #1 (1545), 1284 for sample #2 and the lowest value for sample #3 (1114).

The mean height of shape parameter value is the lowest for sample #1 (13.3 nm), increase for sample #2 (30.8 nm) and increasing trend continue to the highest for sample #3 (35.8 nm).

The mean area of shape parameter has the lowest value for sample #1 (162 nm^2), an average value for sample #2 (195 nm^2) and the highest value for sample #3 (224 nm^2). Similarly, the mean volume parameter has the highest value for sample #3 (127 nm^3) and the lowest value for sample #1 (48.7 nm^3). A decreasing trend from sample #3 to sample #1 is noted for the following parameters: the mean perimeter (57.6 nm, 53 nm, 47.3 nm); the mean of equivalent diameters (13.8 nm, 12.9 nm, 11.5 nm); the mean of mean diameters (13.4 nm, 12.4 nm, 11.2 nm); the mean of minimum diameters (8.3 nm, 7.7 nm, 6.8 nm) and mean of maximum diameter (20.8 nm, 19.1 nm, 17.2 nm).

In other words, the highest values of the mentioned parameters belong to the third sample and the smallest values belong to the first sample, while the second samples have average values.

Sample #1 has the highest value of the mean of minimum diameter angles (−33°), and sample #3 has the lowest value (−36.9°). The highest value of the mean of maximum diameter angles (−27.6°) is found in sample #1, while the lowest value is found in sample #3 (−21.8°). The first sample has the highest mean form factor (0.623) and the lowest mean aspect ratio (2.84). In the case of the third sample, the mean form factor and the mean aspect ratio are 0.604 and 2.90, respectively. The mean orientation parameter increases from sample #1 (79.5°) to sample #3 (84.8°).

For all samples, the number of motifs composed of peaks is more than pits. The density of the peaks of sample #1 is more than others that means that there are many peaks dispersed with a small size and there is no agglomeration observed. It can be noted that sample #1 has the most number of segmented motifs and the lowest values for the following parameters (the mean height, the mean area, and the mean equivalent diameter) that reveal the most regular topography in comparison to other samples.

According to the mean roundness, the mean form factor, the mean aspect ratio and the mean compactness parameters neither of the samples have a form of a disk, therefore all of them are elongated.

Based on statistical results, combined with the average X and Y-PSD profile curves, it can be concluded that the stereometric method is precise and correct applied to analyzed samples.

Conclusions

The numerical stereometric analysis of the 3-D surfaces of the Ag/DLC nanocomposite films fabricated by RF-PECVD method allows us to extend the information about the surface topography related to the time deposition. The applied method can describe the 3-D segmentation of surface samples in motifs (composed of peaks, pits, and irregular shapes) in correlation with ISO 25178-2: 2012. Furthermore, these parameters become more relevant in the defect localization process in various applications. The surface topography measurement and characterization of the Ag/DLC nanocomposite thin films fabricated by sputtering and RF-PECVD technique can lead to a higher understanding of the manufacturing process in correlation with mechanical and physical properties from both experimentally and theoretically.

Declaration of Competing Interest

The authors declare that they have no known competing financial interests or personal relationships that could have appeared to influence the work reported in this paper.

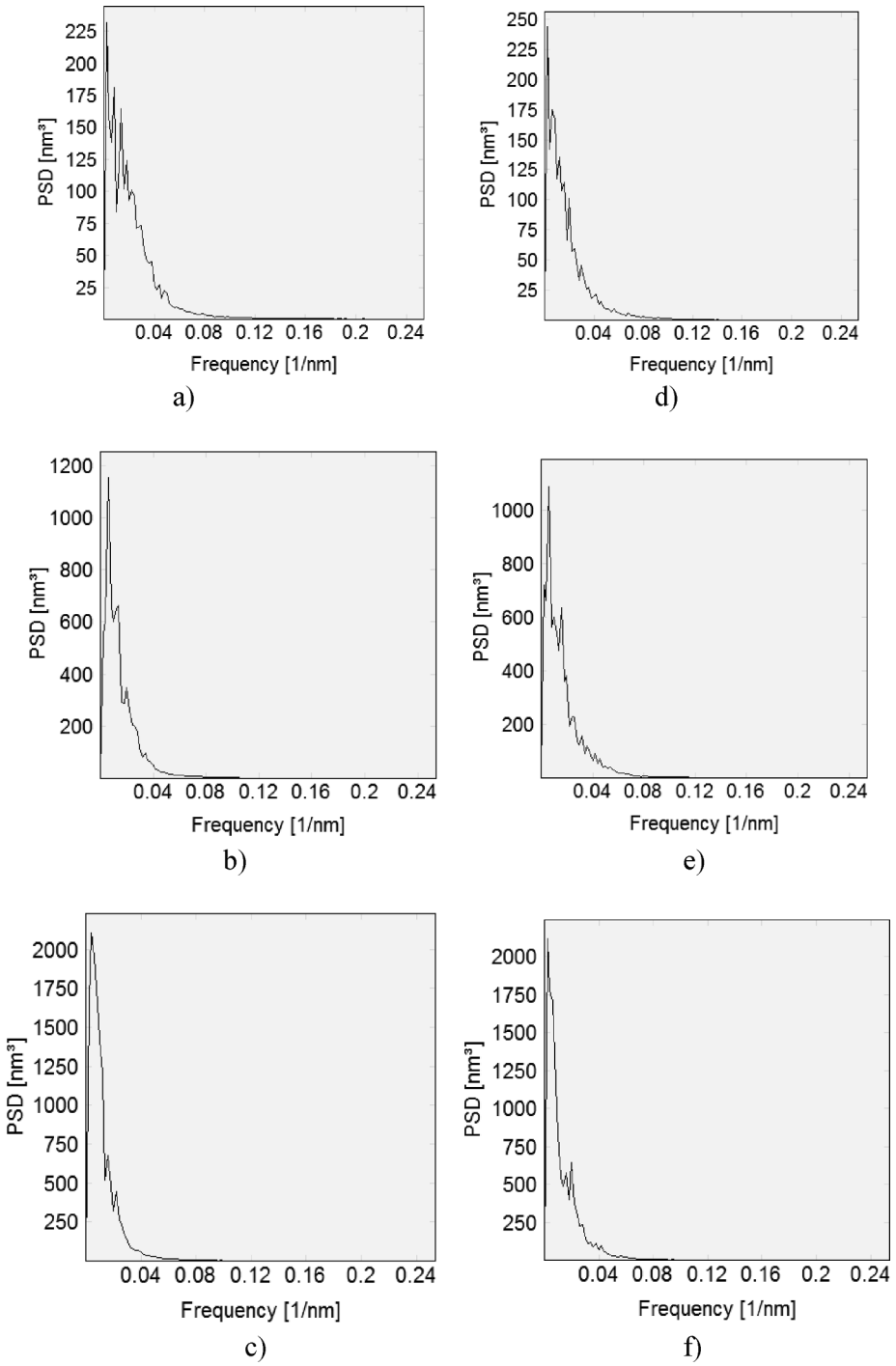

Fig. 5. I) The average X-PSD profile, left column, for: a) #1; b) #2; c) #3; and II) The average Y-PSD profile, right column, for: d) #1; e) #2; f) #3.

Appendix A. Supplementary data

Supplementary data to this article can be found online at https://doi.org/10.1016/j.rinp.2019.102731.

References

[1] Marciano FR, Bonetti LF, Santos LV, Da-Silva NS, Corat EJ, Trava-Airoldi VJ. Antibacterial activity of DLC and Ag–DLC films produced by PECVD technique. Diam Relat Mater 2009;18(5–8):1010–4. https://doi.org/10.1016/j.diamond.2009.02.014.

[2] Wu Y, Chen J, Li H, Ji L, Ye Y, Zhou H. Preparation and properties of Ag/DLC nanocomposite films fabricated by unbalanced magnetron sputtering. Appl Surf Sci 2013;284:165–70. https://doi.org/10.1016/j.apsusc.2013.07.074.

[3] Bociaga D, Komorowski P, Batory D, Szymanski W, Olejnik A, Jastrzebski K, et al. Silver-doped nanocomposite carbon coatings (Ag-DLC) for biomedical applications – Physiochemical and biological evaluation. Appl Surf Sci 2015;355:388–97. https://doi.org/10.1016/j.apsusc.2015.07.117.

[4] Baba K, Hatada R, Flege S, Ensinger W, Shibata Y, Nakashima J, et al. Preparation and antibacterial properties of Ag-containing diamond-like carbon films prepared by a combination of magnetron sputtering and plasma source ion implantation. Vacuum 2013;89:179–84. https://doi.org/10.1016/j.vacuum.2012.04.015.

[5] Constantinou M, Perolaraki M, Nikolaou P, Prouskas C, Patsalas P, Kelires P, et al. Microstructure and nanomechanical properties of pulsed excimer laser deposited DLC: Ag films: enhanced nanotribological response. Surf Coat Technol 2017;309:320–30. https://doi.org/10.1016/j.surfcoat.2016.11.084.

[6] Abdolghaderi S, Astinchap B, Shafiekhani A. Electrical percolation threshold in Ag–DLC nanocomposite films prepared by RF-sputtering and RF-PECVD in acetylene plasma. J Mater Sci: Mater Electron 2016;27:6713–20. https://doi.org/10.1007/s10854-016-4620-4.

[7] Ţălu Ş. Micro and nanoscale characterization of three dimensional surfaces, basics and applications. Cluj-Napoca, Romania: Napoca Star Publishing House; 2015.
[8] Elenkova D, Zaharieva J, Getsova M, Manolov I, Milanova M, Stach S, et al. Morphology and optical properties of SiO_2-based composite thin films with immobilized terbium(III) complex with a biscoumarin derivative. Int J Polym Anal Charact 2015;20:42–56. https://doi.org/10.1080/1023666X.2014.955400.
[9] Ramazanov S, Ţălu Ş, Sobola D, Stach S, Ramazanov G. Epitaxy of silicon carbide on silicon: micromorphological analysis of growth surface evolution. Superlattices Microstruct 2015;86:395–402. https://doi.org/10.1016/j.spmi.2015.08.007.
[10] Arman A, Ţălu Ş, Luna C, Ahmadpourian A, Naseri M, Molamohammadi M. Micromorphology characterization of copper thin films by AFM and fractal analysis. J Mater Sci Mater Electron 2015;26:9630–9. https://doi.org/10.1007/s10854-015-3628-5.
[11] Ţălu Ş, Solaymani S, Bramowicz M, Kulesza S, Ghaderi A, Shahpouri S, et al. Effect of electric field direction and substrate roughness on three-dimensional self-assembly growth of copper oxide nanowires. J Mater Sci Mater Electron 2016;27:9272–7. https://doi.org/10.1007/s10854-016-4965-8.
[12] Stach S, Garczyk Ż, Ţălu Ş, Solaymani S, Ghaderi A, Moradian R, et al. Stereometric parameters of the Cu/Fe NPs thin films. J Phys Chem C 2015;119(31):17887–98. https://doi.org/10.1021/acs.jpcc.5b04676.
[13] Ţălu Ş, Stach S, Ghodselahi T, Ghaderi A, Solaymani S, Boochani A, et al. Topographic characterization of Cu–Ni NPs @ a-C: H films By AFM and multifractal analysis. J Phys Chem B 2015;119(17):5662–70. https://doi.org/10.1021/acs.jpcb.5b00042.
[14] Dallaeva D, Ţălu Ş, Stach S, Škarvada P, Tománek P, Grmela L. AFM imaging and fractal analysis of surface roughness of AlN epilayers on sapphire substrates. Appl Surf Sci 2014;312:81–6. https://doi.org/10.1016/j.apsusc.2014.05.086.
[15] Ţălu Ş, Stach S, Solaymani S, Moradian R, Ghaderi A, Hantehzadeh MR, et al. Multifractal spectra of atomic force microscope images of Cu/Fe nanoparticles based films thickness. J Electroanal Chem 2015;749:31–41. https://doi.org/10.1016/j.jelechem.2015.04.009.
[16] Stach S, Sapota W, Ţălu Ş, Ahmadpourian A, Luna C, Ghobadi N, et al. 3D Surface stereometry studies of sputtered TiN thin films obtained at different substrate temperatures. J Mater Sci Mater Electron 2017;28(2):2113–22. https://doi.org/10.1007/s10854-016-5774-9.
[17] Stach S, Dallaeva D, Ţălu Ş, Kaspar P, Tománek P, Giovanzana S, Grmela L. Morphological features in aluminum nitride epilayers prepared by magnetron sputtering. Mater Sci- Poland 2015;33:175–84. https://doi.org/10.1515/msp-2015-0036.
[18] Naseri N, Solaymani S, Ghaderi A, Bramowicz M, Kulesza S, Ţălu Ş, et al. Microstructure, morphology and electrochemical properties of Co nanoflake water oxidation electrocatalyst at micro- and nanoscale. RSC Adv 2017;7:12923–30. https://doi.org/10.1039/c6ra28795f.
[19] Méndez A, Reyes Y, Trejo G, Stępień K, Ţălu Ş. Micromorphological characterization of zinc/silver particle composite coatings. Microsc Res Tech 2015;78:1082–9. https://doi.org/10.1002/jemt.22588.
[20] Sobola D, Ţălu Ş, Solaymani S, Grmela L. Influence of scanning rate on quality of AFM image: study of surface statistical metrics. Microsc Res Tech 2017;80. https://doi.org/10.1002/jemt.22945.
[21] Ţălu Ş, Bramowicz M, Kulesza S, Solaymani S, Shafikhani A, Ghaderi A, et al. Gold nanoparticles embedded in carbon film: micromorphology analysis. J Ind Eng Chem 2016;35:158–66. https://doi.org/10.1016/j.jiec.2015.12.029.
[22] Solaymani S, Kulesza S, Ţălu Ş, Bramowicz M, Nezafat NB, Dalouji V, et al. The effect of different laser irradiation on rugometric and microtopographic features in zirconia ceramics: study of surface statistical metrics. J Alloy Compd 2018;765:180–5. https://doi.org/10.1016/j.jallcom.2018.06.213.
[23] Smagoń K, Stach S, Ţălu Ş, Arman A, Achour A, Luna C, et al. Studies of the micromorphology of sputtered TiN thin films by autocorrelation techniques. Eur Phys J Plus 2017;132:520. https://doi.org/10.1140/epjp/i2017-11801-5.
[24] Zavarian AA, Ţălu Ş, Hafezi F, Achour A, Luna C, Naderi S, et al. Study of the microstructure and surface morphology of silver nanolayers obtained by ion-beam deposition. J Mater Sci Mater Electron 2017;28(20:15293–301. https://doi.org/10.1007/s10854-017-7410-8.
[25] Ţălu Ş, Stach S, Mahajan A, Pathak D, Wagner T, Kumar A, et al. Multifractal analysis of drop-casted copper (II) tetrasulfophthalocyanine film surfaces on the indium tin oxide substrates. Surf Interface Anal 2014;46(6):393–8. https://doi.org/10.1002/sia.5492.
[26] ISO 25178-2: 2012, Geometrical product specifications (GPS) – Surface texture: Areal - Part 2: Terms, definitions and surface texture parameters. Available from: http://www.iso.org (last accessed 10.10.2018).
[27] MountainsMap® Premium software (Digital Surf, Besançon, France). Available from: http://www.digitalsurf.fr (last accessed 10.10.18).
[28] SPIP™ 6.7.4 software (Copyright ® 1998-2018 Image Metrology A/S). Available from: http://www.imagemet.com (last accessed 10.10.18).